
Predicting the Impact of Model Expansion through the Minima Manifold: A Loss Landscape Perspective

Pranshu Malviya
Mila - Québec AI Institute
Polytechnique Montréal

Jerry Huang
Mila - Québec AI Institute
Université de Montréal

Quentin Fournier
Mila - Québec AI Institute

Sarath Chandar
Mila - Québec AI Institute
Polytechnique Montréal
Canada CIFAR AI Chair

Abstract

The optimal model for a given task is often challenging to determine, requiring training multiple models from scratch which becomes prohibitive as dataset and model sizes grow. A more efficient alternative is to reuse smaller pre-trained models by expanding them, however, this is not widely adopted as how this impacts training dynamics remains poorly understood. While prior works have introduced statistics to measure these effects, they remain flawed. To rectify this, we offer a new approach for understanding and quantifying the impact of expansion through the lens of the loss landscape, which has been shown to contain a manifold of linearly connected minima. Building on this new perspective, we propose a metric to study the impact of expansion by estimating the size of the manifold. Experimental results show a clear relationship between gains in performance and manifold size, enabling the comparison of candidate models and presenting a first step towards expanding models more reliably based on geometric properties of the loss landscape.

1 Introduction

Neural network size greatly affects performance, with several works suggesting that as training datasets grow, one can scale models and train them from scratch for improved performance [Kaplan et al., 2020]. Yet this approach is computationally expensive, and a more efficient approach would be to reuse smaller existing models by expanding them. Expansion enables knowledge transfer [Chen et al., 2016, Wang et al., 2023], but despite its usefulness, it remains a poorly understood process that can lead to sub-optimal performance if done haphazardly, hence necessitating further training the expanded models. Thus building a link between how a model is expanded and its final performance on a given task is of crucial importance, as otherwise significant resources can be misspent.

Several metrics have been proposed to predict the final performance of a model using only information from partially trained candidates [White et al., 2023]. However, the increasing scale of models necessitates that the information is (i) reliable and independent of the overall optimization process and (ii) cost-effective to obtain. Existing methods often fall short on one of these fronts. Informative statistics are typically challenging to compute or require further training the expanded model, while low-cost information is often inconsistent and unreliable [White et al., 2021b]. It follows that better metrics are needed for informed decisions, but obtaining them remains an open issue.

Properties of the loss surface are a popular source of information to optimize neural networks and their architecture. Indeed, several studies have demonstrated that incorporating information from the

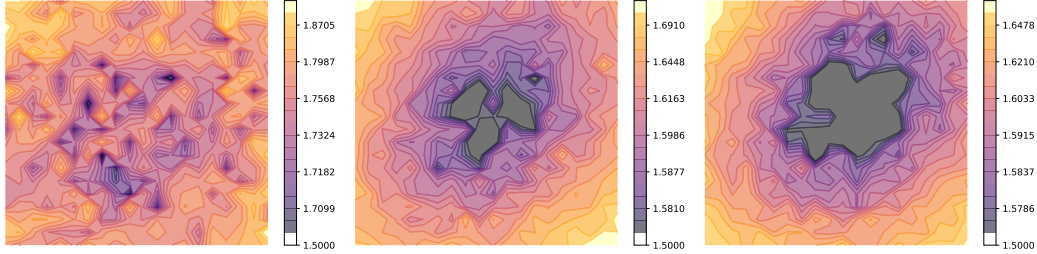


Figure 1: LMC between minima using a MLP with one hidden layer (20 units) pre-trained on CIFAR10. The initial model (first) is expanded by increasing the hidden layer size in a function-preserving way and trained further until convergence. Final models after hidden size expansions of $2\times$ (second) and $3\times$ (third) show a reduced loss and enhanced local connectivity between minima.

local loss landscape can significantly improve the optimization process [Foret et al., 2021, Liu et al., 2022]. The loss landscape is determined by two important aspects: the architecture of the model and the distribution of the training data [Cooper, 2018]. Both aspects play a crucial role in determining the model’s final performance, and the loss function thus holds a wealth of intrinsic information [Li et al., 2018, Li and Spratling, 2023]. Analyzing or even estimating the properties of the loss landscape can therefore provide essential insights into the entire training process. We subsequently ask:

Is it possible to understand and quantify the impact of model expansion from the perspective of the loss landscape?

Empirical findings hint that geometric properties hold the answer. First, Sun [2019] suggests that the loss landscapes of high-dimensional models exhibit non-trivial properties that can identify how easy the optimization is. One such property, linear mode connectivity (LMC), indicates that the minima obtained from models trained with different initialization can be connected via linear or low-loss paths [Garipov et al., 2018, Frankle et al., 2020, Anokhin and Yarotsky, 2020]. Entezari et al. [2021] and Ainsworth et al. [2022] further show the emergence of this connectivity between multiple minima when permuting the model parameters in a function-preserving way. Finally, Benton et al. [2021] and Simsek et al. [2021] noted the presence of a manifold connecting such minima via low-loss paths.

Based on these observations, we argue that connectivity plays a crucial role in understanding how the loss landscape changes when a network is expanded, as well as how its final performance is affected. To illustrate this, Figure 1 shows how the manifold size increases when a small network is expanded along its width. This inspires us to design a metric based on local connectivity, using the difference in the size of the minima manifold to compare candidate expansions.

Using this metric, we conduct a series of experiments on models and benchmarks frequently used to study the properties of the loss landscape from a theoretical perspective [Simsek et al., 2021, Wang et al., 2022, Zhou et al., 2023]. However, while these empirical analyses had previously remained limited to multi-layer perceptrons (MLPs) and convolutional neural networks (CNNs), we also evaluate Transformers [Vaswani et al., 2017], which have been shown to possess highly different optimization characteristics [Yang et al., 2021]. We summarize our contributions as follows:

- We examine the impact of model expansion on the loss landscape to estimate performance gain in high-dimensional neural networks.
- We conduct image classification experiments and reveal an increase in the manifold size as the model is expanded, and consequently, the metric is a more robust and representative predictor of performance gain compared to existing baselines, highlighting its practical use.
- We conduct language modeling experiments and reveal a significant reduction in manifold size as Transformers are pre-trained, suggesting that Transformers may not exhibit the same LMC properties as CNNs.

2 Related work

Neural Network Expansion. Expansion can reduce the computational cost of training neural networks by re-using smaller pre-trained models. Furthermore, many real-world applications are continuous by nature [Douillard et al., 2022] and thus require that the capacity of the model increases to allow learning over multiple datasets [Li et al., 2019]. Accordingly, several expansion strategies have been explored in deep learning. Fahlman and Lebiere [1989] and Gutstein et al. [2008] added hidden units and layers respectively, but kept existing parameters frozen, limiting learning to the new parameters. Meanwhile, Chen et al. [2016] introduced a function-preserving expansion method for MLPs and CNNs, called Net2net, that keeps existing units trainable. More recently, numerous strategies have been explored for Transformers as well [Gong et al., 2019, Gu et al., 2021, Wang et al., 2023, Gesmundo and Maile, 2023]. Nonetheless, these methods lack a mechanism to assess whether expanding the model will yield an improvement and provide no signal regarding how or by how much to expand. Unlike these prior works, we do not introduce a new expansion method; instead, we introduce a flexible and inexpensive way to easily estimate the impact of expansion on the model’s generalization.

Finding Optimal Models with Performance Prediction. While finding the optimal model among many is complex, advances have been made. Most notably, neural architecture search (NAS) [Zoph and Le, 2017] automates the process of finding the best-performing model by conducting an automatic search over a space of architecture and ranking them by predicting their performance on a task [Ren et al., 2021]. Furthermore, numerous techniques have been explored to predict the final performance of a model after expansion. White et al. [2021b] introduced a taxonomy that includes the following categories. Model-based methods train several candidate models to construct a dataset to train a parameterized predictor model, thereby requiring large initialization times [Springenberg et al., 2016, Siems et al., 2020, White et al., 2021a]. Learning curve extrapolation methods rely on partially trained candidate models to predict the final performance and, therefore, exhibit high query times [Ru et al., 2020, Zoph et al., 2018]. Zero-cost proxies provide estimates of the (relative) performance of neural architectures from a small amount of data [Mellor et al., 2021, Lee et al., 2018, Wang et al., 2020, Tanaka et al., 2020]. Our method belongs to the zero-cost proxies and uses the local loss landscape for making predictions.

Properties of the Loss Landscape. Several known metrics allow characterizing the properties of the loss landscape, some of which have been employed for NAS [Abdelfattah et al., 2021, White et al., 2021b, Mellor et al., 2021, Kaur et al., 2023, Shen et al., 2023]. However, these metrics can be highly dependent on the optimization process and location of parameters. In contrast, metrics that estimate the geometric properties of the loss landscape inherently mitigate this dependency. The manifold size is one such geometric property that has gained interest [Kunin et al., 2019]. In particular, Simsek et al. [2021] mentioned that, since permutation symmetries give rise to several equivalent global minima, expanding a model by width is sufficient to connect these global minima into a single manifold, which could be the key to converging to the global minima. Therefore, it is important to validate the presence of such a manifold in a trained model [Wu et al., 2018, Fort et al., 2020].

3 Methodology

This section describes our proposed metric for estimating the benefit of expansion by quantifying changes in the loss landscape, and more specifically, the size of the manifold.

3.1 Linear Mode Connectivity

Our metric relies on the LMC between minima measured using the loss barrier [Entezari et al., 2021] defined below.

Definition 1 (Loss Barrier). *Consider two networks with parameters $\theta_1, \theta_2 \in \mathbb{R}^k$ and a loss function \mathcal{L} evaluated on a dataset \mathcal{D} . The **loss barrier** $b(\theta_1, \theta_2)$ along the linear path between θ_1 and θ_2 is defined as the greatest difference between the loss of the linear interpolation between the two networks and the linear interpolation between their losses:*

$$b(\theta_1, \theta_2) = \sup_{\alpha} \mathcal{L}(\alpha\theta_1 + (1 - \alpha)\theta_2) - [\alpha\mathcal{L}(\theta_1) + (1 - \alpha)\mathcal{L}(\theta_2)] \tag{1}$$

where $\alpha \in [0, 1]$ determines the location on the linear path.

More intuitively, different configurations exist along the linear interpolation between two network configurations θ_1 and θ_2 . If, at any point along this path, the true loss value differs from the hypothetical loss value assuming a linear path, a *barrier* blocks the path between the two network configurations in the loss surface. The two networks are said to be linearly connected if their loss barrier is zero.

3.2 Manifold Detection

Entezari et al. [2021] and Ainsworth et al. [2022] proposed search algorithms to find the permutation that minimizes the loss barrier (Equation 1) with the goal of aligning the weights of two independently trained models. In contrast, we propose an algorithm to detect the presence of a manifold within a given model. We define a manifold as a graph whose nodes represent distinct models generated by permutations of a base model trained to convergence and whose edges indicate LMC between two permutations with a relaxed linearity constraint.

For a model parameterized by $\theta \in \mathbb{R}^k$, we obtain a new parameter configuration θ_{perm} by randomly permuting neurons in θ such that both lie in functionally equivalent regions [Kuditipudi et al., 2019, Peña et al., 2023]. If \mathbf{P}_θ represents the set of permutations that produce functionally equivalent parameters to θ , then the permutation function is given by $P : \mathbb{R}^k \times \mathbf{P}_\theta \rightarrow \mathbb{R}^k$.

As our algorithm depends on the linearity of the connection, we use the absolute value to define $\hat{b}(\theta) = |b(\theta, P(\theta, \pi))|$ as the loss barrier where $\pi \sim \mathbf{P}_\theta$. Following Yang et al. [2021], we compute the loss barrier at the mid-point by setting $\alpha = 0.5$. Given a model θ , maximum number of permutations n and threshold λ , our algorithm is as follows:

- (i) Iteratively generate n random permutations of the base node θ .
- (ii) For each new node i , check if there exists an edge between the current node and the previous node by satisfying the linearity constraint, i.e., $\hat{b}_i(\theta) \leq \lambda$.
- (iii) Return the ratio $m(\theta, \lambda, n)$ between the number of edges in the graph (e) and the maximum number of possible edges (e_{upper}), i.e., $m(\theta, \lambda, n) = \frac{e}{e_{\text{upper}}}$

If the nodes are permutation invariant, the resulting loss barrier is small and the minima are considered *connected* in the manifold. A dense graph indicates a large manifold and results in $m(\theta, \lambda, n) \approx 1$.

Unlike Entezari et al. [2021], we compute the loss barrier only between two consecutive nodes and ensure that the highest degree in the generated graph remains 2. This mitigates the use of a *bad* node i.e., a node not connected to any other nodes that would otherwise result in a reduction of the upper bound e_{upper} from ${}^n C_2$ to $[{}^n C_2 - (n - 1)]$. The iterative generation of nodes approach also reduces the algorithmic complexity from $O(n^2)$ to $O(n)$, as $e_{\text{upper}} = n$ corresponds to the number of forward passes required to compute the metric. We provide the pseudo-code in Algorithm 1. Using this algorithm, we define our manifold metric for evaluating model expansion in the next section.

Algorithm 1 Manifold detection: $m(\theta, \lambda, n)$

Require: Model \mathcal{M}_θ , Number of nodes n , Threshold λ , Loss function L_D
 $e \leftarrow 0, \theta_1 \leftarrow \theta$
for i in $[1, n]$ **do**
 Sample π_i from \mathbf{P}_θ without replacement
 $\theta_{i+1} \leftarrow P(\theta, \pi_i)$ \triangleright Permuted model
 $\hat{b}_i(\theta) \leftarrow |b(\theta_i, \theta_{i+1})|$ \triangleright Equation 1
 if $\hat{b}_i(\theta) \leq \lambda$ **then** $e \leftarrow e + 1$
 $\theta_i \leftarrow \theta_{i+1}$
end for
return e/n

3.3 Permutation Invariance and Expansion

Let the parameters of the pre-trained base model be ϕ^* . We perform a function-preserving expansion $\phi^* \rightarrow \theta$ using Net2net [Chen et al., 2016] to initialize new parameters. To ensure a fair evaluation of model expansion, we fix n and λ throughout the process. Here, n determines the size of the graph, with higher values leading to a better estimate of the manifold at the cost of more computations. On the other hand, λ dictates the strictness of the connection between two minima to be linear, with smaller values enforcing stronger linearity constraints. The manifold size of a candidate model

hence depends on the λ associated with the base model. Accordingly, we define a set of loss barriers between permutations i.e., $B^* = \{\hat{b}_i(\phi^*) : i \in [1, n]\}$ and define $\lambda = B_q^*$, i.e., the q^{th} quantile of B^* where $q \in (0, 1)$. We evaluate expansion using the manifold metric M defined as:

$$M(\theta, \phi^*) = m(\theta, B_q^*, n) - m(\phi^*, B_q^*, n) \quad (2)$$

Although $M(\theta, \phi^*)$ primarily indicates changes in the geometric properties of the loss landscape, several other factors can influence its behavior. In particular, curvature matters since if the parameter lies on a sharp or noisy surface, the algorithm would find fewer edges, i.e., the optimal q would be higher. Alternatively, if the pre-trained base model is already over-parameterized or contains dead neurons, B_q^* will be smaller and the resulting metric may not indicate any change in the manifold size after the expansion, even if there is a gain in performance.

4 Experiments

4.1 Setup

In order to evaluate the manifold metric on model expansion, we first train a small base model with parameters ϕ until early stopping, at which point the parameters have evolved to ϕ^* . We record the best validation performance as $A(\phi^*)$. The first layer of the model is expanded to obtain a new set of parameters $\theta^{(0)}$ such that $A(\theta^{(0)}) = A(\phi^*)$, i.e. the expansion is function-preserving. We compute the manifold metric $M(\theta^{(0)}, \phi^*)$ using Equation 2 (as a percentage). For simplicity, we refer to $M(\theta^{(t)}, \phi^*)$ as M_t for the remainder of this work. The expanded model is trained for an additional T epochs to obtain a performance gain $G_T = A(\theta^{(T)}) - A(\phi^*)$, where $\theta^{(t)}$ denotes the parameters after training the expanded model for $t \in [0, T]$ epochs. Although the first layer may appear specific, permuting these neurons can lead to a substantial shift in the parameter location, which is crucial for determining the geometry of the loss landscape [Zhang et al., 2022].

We run our experiments with CNNs on CIFAR10/100, ResNet18 He et al. [2016] on CIFAR10, and TinyBERT/MiniBERT [Devlin et al., 2019] on WikiText-103 [Merity et al., 2016]. Unless specified, hyper-parameters were determined with a grid search, detailed in Appendix A.2.2. CNNs/ResNets are expanded along the width/channels, and BERT models along the width of the intermediate layer in the feed-forward network. Permutations are also conducted along these specific axes (Appendix A.2.1). All results are averaged across 10 seeds and presented along with the standard deviation.

4.2 Comparison with Zero-Cost Baselines

Our proposed metric does not require resuming training; we therefore start by comparing the manifold metric with several zero-cost proxy baselines that include gradient norm (GradNorm) [Chen et al., 2018], Jacobian covariance (Jacov) [Mellor et al., 2021], and pruning-based methods like single-shot network pruning (SNIP) [Lee et al., 2018], gradient signal preservation (Grasp) [Wang et al., 2020], and synaptic flow (SynFlow) [Tanaka et al., 2020] that have previously been adapted as zero-cost proxies by Abdelfattah et al. [2021]. Among these baselines, Jacov and SynFlow have shown a high correlation with performance [White et al., 2021b]. We ensure that our metric and the baselines use a fixed number of training examples i.e., a single batch of the training data for their computation.

Results in Figure 2 show the correlation between the metrics and the highest performance gain G_T^* observed after expanding pre-trained models and training them for at least T epochs. We use Kendall Tau rank correlation [Puka, 2011] throughout our experiments following White et al. [2021b]¹. The manifold metric is the *only* metric that remains positively correlated for all settings, while the selected baselines can vary, making them unreliable as general-purpose metrics across the chosen benchmarks. This showcases the consistency and reliability of manifold metrics in ranking candidate models for expansion without training, as it remains best or competitive to the second-best baseline. Meanwhile, SynFlow shows a high correlation with performance in 3 out of 5 settings and Jacov shows a low correlation that remains close to 0, suggesting that unlike in NAS, their performance remains poor and inconsistent when evaluated on pre-trained model expansion.

A detailed comparison between the manifold metric and baselines in terms of computation time is presented in Appendix A.2.3. We also provide a sensitivity analysis in §4.5 and Appendix A.2.5

¹Similar results using Spearman and Pearson rank correlation metrics are presented in Appendix A.2.4.

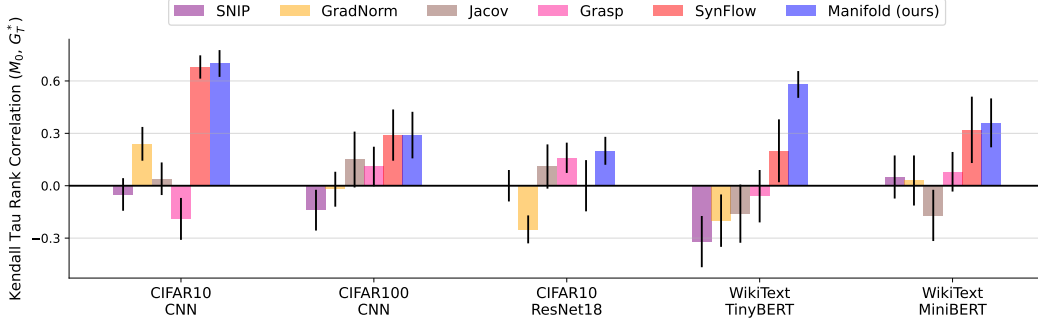


Figure 2: Comparison between our manifold metric and existing zero-cost proxies in terms of Kendall Tau rank correlation with the performance gain G_T^* . The horizontal axis indicates the dataset and the base model. Correlation with our metric remains consistently positive and competitive to the second-best baseline, whereas other baselines fluctuate between positive and negative.

that shows a trend in the correlation obtained by varying n and q . In almost all cases, increasing n improves the overall representative power of the metric for estimating the change in manifold size. Moreover, we find that it is possible to obtain an optimal value for the threshold quantile q without running an exhaustive grid search.

4.3 Image Classification

To analyze changes in the loss landscape when training an expanded model, we compare our manifold metric with the sum of training losses per epoch (SoTL-E) [Ru et al., 2021], which has been shown to have a high correlation with final validation accuracy in NAS literature [White et al., 2021b]. In the following experiments, we track the performance gain G_t and the manifold metric M_t for $(q, n) = (0.4, 1000)$. We also present a brief sensitivity analysis in terms of correlation between M_t and G_T^* for $q \in \{0.1, 0.2, 0.4\}$.

Figure 3 reveals that when training expanded CNNs on CIFAR10 (first row), increasing the number of channels results in larger performance gain (first column), and the manifold metric is positively correlated (second and third columns). We also observe that $q = 0.4$ performs marginally better than lower values of q . On CIFAR100 (second row), over-fitting occurs at the end of training and G_t improves marginally with an increasing number of channels, resulting in an overlap of overall performance gains. As a result, the correlation is initially small but positive.

For both datasets, M_t remains constant in the beginning (up to $t \approx 20$) and drops during the later phase of training. This observation indicates that nodes generated by randomly permuting $\theta^{(t)}$ for $t \leq 20$ can be connected via linear paths more often. But when the model is trained further, the parameters enter a sharper region in the loss landscape with higher barrier sizes and therefore result in smaller $m(\theta^{(t)}, \lambda, n)$ in Equation 2. For instance, in CIFAR100 for $q = 0.4$ (and therefore $m(\phi^*, \lambda, n) \approx 40$), $m(\theta^{(t)}, \lambda, n)$ approaches 0 when over-fitting occurs for $t \geq 200$ and, as a result, we observe $M_t \approx -40$.

We also observe that SoTL-E initially results in a highly negative correlation, which suggests SoTL-E can correlate well to the performance gain at a given epoch G_t rather than the final performance gain G_T^* . While SoTL-E is considered an oracle scoring method, its effectiveness appears to be highly dependent on the current parameter location, which is undesirable as these baselines could require training the candidate models of expansion for extended (high query) time before accurately ranking them [White et al., 2023]. Therefore, even when we train the expanded model, the manifold metric can provide an approximate rank for generalization performance earlier on.

4.3.1 Ablations on CNN Expansion

In the previous results, we expanded the base CNN model by adding more channels in its first layer. To highlight our method’s robustness to the expansion being performed, we provide an ablation study where we (i) expand width in all CNN layers on CIFAR100, (ii) increase depth of the CNN model on

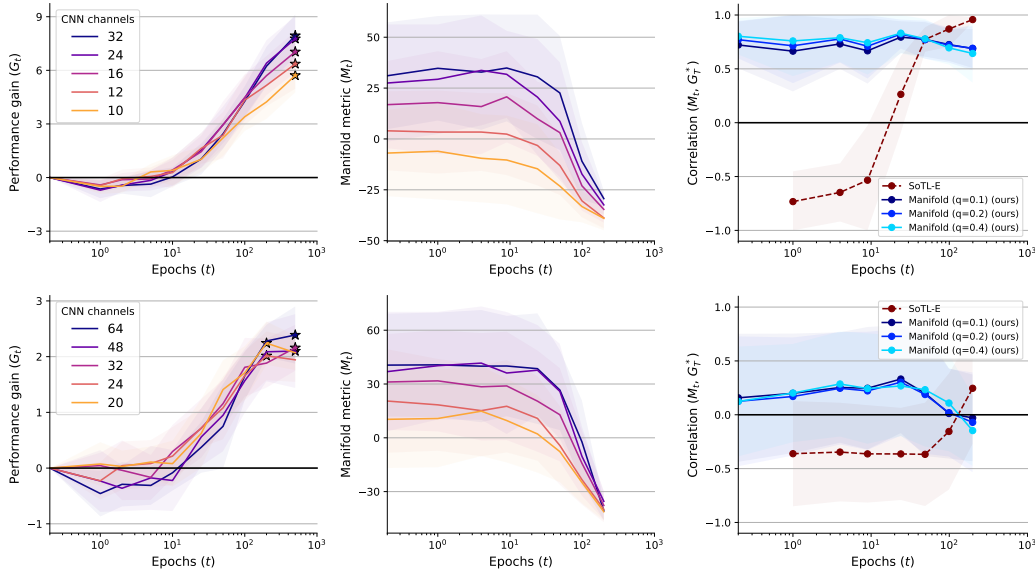


Figure 3: Performance gain G_t (first column; \star denotes the best performance gain G_T^*), manifold metric M_t (second column) and correlation between M_t and the highest gain G_T^* (third column) on expanding and training CNN on CIFAR10 (top) or CIFAR100 (bottom) for $T = 500$ epochs. Overall, M_t remains constant and proportional to G_T^* from the beginning and drops during the later phase of training. Comparison of correlations shows that SoTL-E is correlated to the gain G_t at a given epoch t and therefore results in a negative correlation with G_T^* initially. Our manifold metric positively correlates early on, making it more reliable for comparing expanded models.

CIFAR100, and (iii) expand a ResNet18 model [He et al., 2016] by width on CIFAR10. We use the same CNN model from the previous section for CIFAR100 ablations. We also use Net2net [Chen et al., 2016] for initializing new parameters so that the expansion is function-preserving. We set $q = 0.4$ and $n = 1000$ in all three setups.

When increasing the width of all the convolutional layers, Figure 4 (first column) shows the performance gain to be similar for all expansion factors, but M_t attains an overall positive correlation early on during training. We also observe that when the number of channels is increased up to 24, the increase in M_t is more pronounced. Interestingly, in this case, M_t increases in the first few epochs, instead of remaining constant, before decreasing for later epochs. During depth expansion (second column) for the same base model, adding more layers results in increasing performance. In this case, while the manifold metric correlates with G_T^* on average, there is significant overlap across different levels of expansion. When expanding the convolutional layers in a ResNet18 model (third column) by width, while there is a variance overlap in M_t , it remains positively correlated to G_T^* .

4.4 Language Modeling

While the existence of LMC in the loss surfaces of MLPs and CNNs has been broadly explored, understanding of the loss landscape geometry in Transformers remains limited [Yang et al., 2021]. Nevertheless, Qin et al. [2022] suggested that LMC emerges during fine-tuning, where a pre-trained model is evaluated on different tasks, motivating us to study the manifold metric with encoder-only Tiny/MiniBERT models, specifically with masked language modeling on WikiText-103. We train a base model for 5 epochs before expansion, then expand the model by increasing the intermediate layer width of its feed-forward networks. The expanded model is further trained for 15 epochs, with the performance measured as a negative log of validation loss.

Figure 5 (first column) shows that increasing the FFN width in both TinyBERT and MiniBERT contributes to performance gain. However, there is an initial increase in the manifold size followed by a significant drop as the model is trained after expansion (second column), which is interesting. While several plausible reasons for this exist, we include two ablations in Appendix A.2.7 to verify whether this phenomenon specifically occurs because of the expansion: we (i) train a Transformer

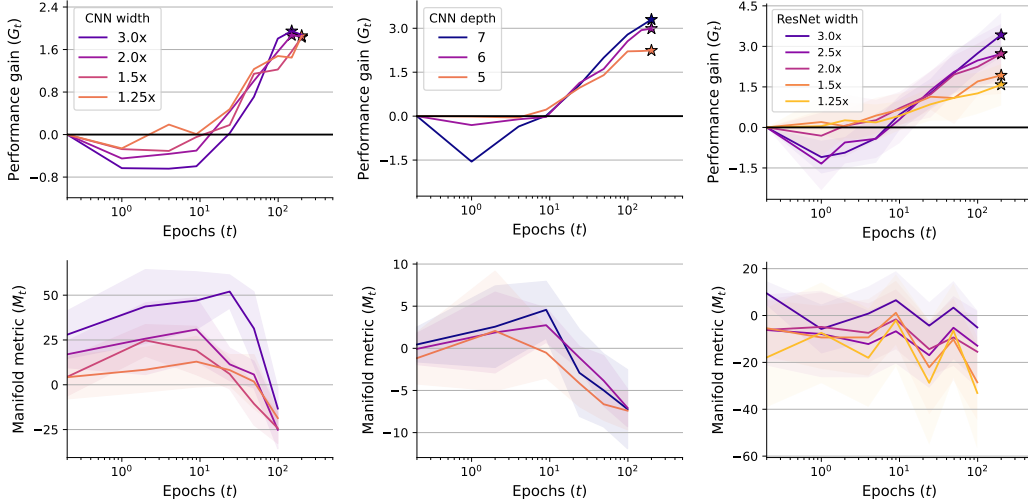


Figure 4: Performance gain G_t (first row; \star denotes the best performance gain G_t^*) and manifold metric M_t (second row) for CNN width expansion on all layers (first column), CNN depth expansion on CIFAR100 (second column), and ResNet width expansion on CIFAR10 (third column). Our manifold metric positively correlates with the level of expansion.

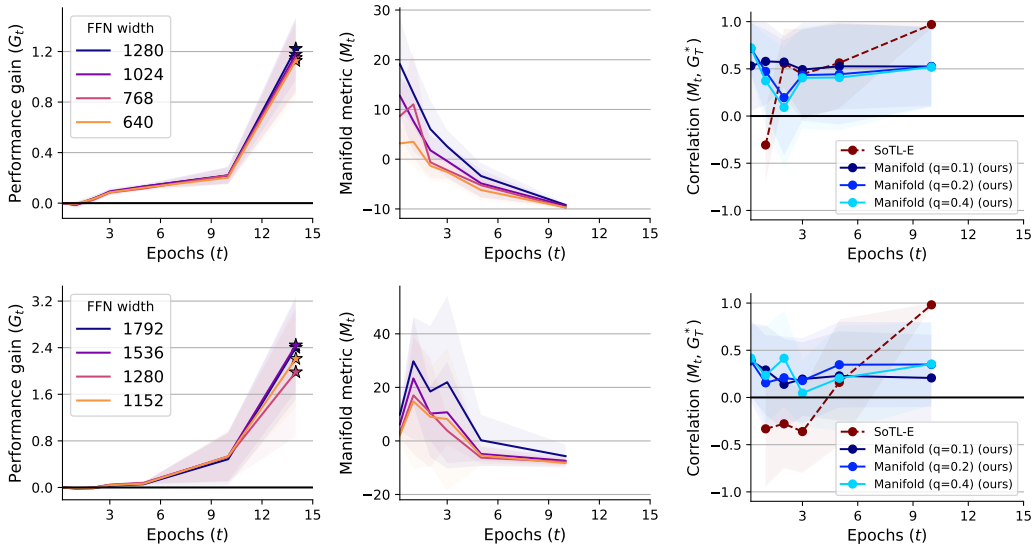


Figure 5: Performance gain G_t (first column; \star denotes the best performance gain G_T^*), manifold metric M_t (second column) and correlation between M_t and the highest gain G_T^* (third column) for FFN expansion in TinyBERT (first row) and MiniBERT (second row) on WikiText-103 dataset. The manifold size drops as the expanded model is trained, but the manifold metric M_t remains positively correlated with G_T^* . However, SoTL-E shows a negative correlation at the start of training.

from a random initialization and (ii) permute self-attention weights instead of FFN weights. Both cases observe a similar drop in the manifold size, suggesting a link with the overall training dynamics in the Transformer and language modeling tasks. Despite the drop, a positive correlation still exists throughout training after expansion for both BERT models. This is crucial since SoTL-E begins with a negative correlation and takes at least 2 epochs to show a positive correlation.

4.5 Sensitivity Analysis

This section presents sensitivity analysis results obtained by performing a grid search over the sets q and n . The goal of such an analysis is to show the robustness of our manifold metric M_0 across different optimization settings and models by calculating the Kendall Tau correlation with the final performance gain G_T^* for various combinations of (q, n) .

Figure 6 illustrates the average correlation obtained over 10 different seeds for the following settings: expanding a CNN model pre-trained on CIFAR10 using Adam (first), AdamW (second), and expanding a TinyBERT model pre-trained on Wikitext-103 using AdamW (third). For all combinations of (q, n) in all three cases, the manifold metric results in a positive correlation. More importantly, higher values of n result in higher correlation, which suggests that more accurate estimates of the manifold size can indeed lead to better correlation with the performance gain. Additionally, for both CNN and TinyBERT models pre-trained using AdamW, a higher value of q tends to result in better correlation. A similar pattern occurs in CNN with Adam, despite less pronounced trends, where a smaller $q = 0.05$ also results in a high correlation.

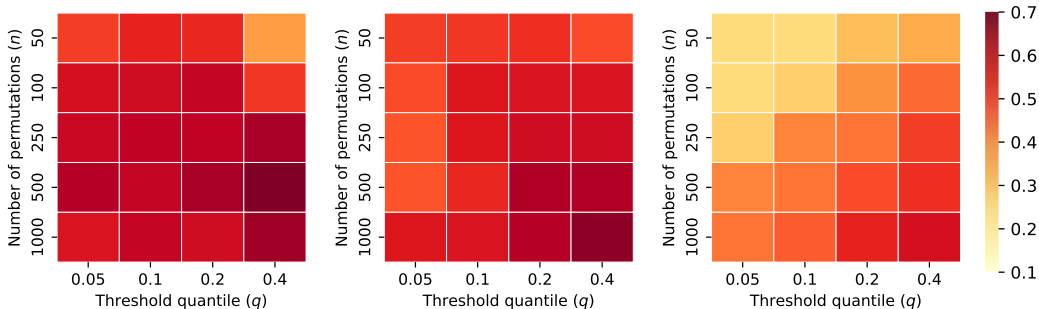


Figure 6: Sensitivity analysis on CNN on CIFAR10 with Adam (first), AdamW (second) and TinyBERT on WikiText-103 with AdamW (third), in terms of Kendall Tau correlation observed between the manifold metric M_0 and the overall performance gain G_T^* . We observe that correlation generally increases as we grow the number of permutations n and threshold quantile q .

These findings suggest that the change in manifold size serves as a reliable estimator of potential performance gain when expanding a pre-trained model. Furthermore, a high optimal q indicates that this estimation does not rely explicitly on the linearity of connections between minima. Rather, as long as the minima are connected through low-loss paths, the change in manifold size can predict the impact of expansion on overall performance.

5 Discussion and Limitations

Throughout this work, we observed that model expansion can lead to an overlap in performance gain across seeds for different expansion factors. For example, in CNN width expansion on CIFAR100, the difference between G_T^* for different expansion factors was almost similar. Despite this, M_t continues to consistently exhibit a positive and a higher correlation with G_T^* as compared to all other baselines. Therefore, even when there is significant variance in performance or correlation, the metric is sufficient to make a personalized choice on whether to continue expansion or not.

Our experiments mainly focused on expanding small-scale models such as CNNs and TinyBERT. However, our results indicate that the manifold metric is more reliable compared to other baselines as both model and dataset complexity increase, serving as a promising starting point. Our sensitivity analysis on these setups also suggests a trend that leads to better correlation as we increase the number of permutations and threshold quantiles, allowing one to avoid running an exhaustive grid search over these hyperparameters potentially. While similar experiments could be conducted on large-scale models using alternative techniques, such as expanding the hidden dimensions or increasing depth in a BERT model, we leave this direction for future work.

While different initialization methods exist for the newly added parameters after expansion, we use Net2net [Chen et al., 2016] in our experiments. Since the manifold size requires the parameters to be

located at a minimum in the loss landscape, exploring different initialization methods is orthogonal to our experiments as long as the function is preserved after expansion.

6 Conclusion

In this paper, we observe the effects of expanding a model through the perspective of the loss landscape. We introduce a metric that estimates the size of the minima manifold and shows that it can reliably evaluate the benefits of model expansion. Our results indicate that this metric can correctly rank models for image classification tasks, unlike other existing baselines, without requiring training the model for several epochs. Experiments with Transformers suggest that expansion can lead to a more complex and non-linear loss landscape, which comes with a significant drop in manifold size that underscores the limited understanding of their training dynamics.

The applications of the proposed metric are not limited to architecture search. It evaluates whether any change in the loss landscape results in an increase in manifold size and since changes in data distributions also result in changes in the loss landscape, we believe it helps evaluate whether a given model can perform well under distribution shifts. Therefore, we believe that such metrics can be useful for continual learning, online learning, and out-of-distribution generalization, among others. We hope that these promising directions can be explored in future work.

7 Acknowledgements

Pranshu Malviya is partially supported by the Merit scholarship program for foreign students (PBEEE) by Fonds de Recherche du Québec Nature et technologies (FRQNT). Jerry Huang is partially supported by a Natural Sciences and Engineering Research Council of Canada (NSERC) Canada Graduate Scholarship, FRQNT training scholarship and Hydro-Québec Excellence Scholarship. Sarath Chandar is supported by the Canada CIFAR AI Chairs program, the Canada Research Chair in Lifelong Machine Learning, and the NSERC Discovery Grant. This research was enabled in part by compute resources provided by Mila (mila.quebec) and the Digital Research Alliance of Canada (alliancecan.ca).

References

- Mohamed S Abdelfattah, Abhinav Mehrotra, Łukasz Dudziak, and Nicholas D Lane. Zero-cost proxies for lightweight nas. *arXiv preprint arXiv:2101.08134*, 2021.
- Samuel K Ainsworth, Jonathan Hayase, and Siddhartha Srinivasa. Git re-basin: Merging models modulo permutation symmetries. *arXiv preprint arXiv:2209.04836*, 2022.
- Ivan Anokhin and Dmitry Yarotsky. Low-loss connection of weight vectors: distribution-based approaches. In *International Conference on Machine Learning*, pages 335–344. PMLR, 2020.
- Gregory Benton, Wesley Maddox, Sanae Lotfi, and Andrew Gordon Gordon Wilson. Loss surface simplexes for mode connecting volumes and fast ensembling. In Marina Meila and Tong Zhang, editors, *Proceedings of the 38th International Conference on Machine Learning*, volume 139 of *Proceedings of Machine Learning Research*, pages 769–779. PMLR, 18–24 Jul 2021. URL <https://proceedings.mlr.press/v139/benton21a.html>.
- James Bradbury, Roy Frostig, Peter Hawkins, Matthew James Johnson, Chris Leary, Dougal Maclaurin, George Necula, Adam Paszke, Jake VanderPlas, Skye Wanderman-Milne, and Qiao Zhang. JAX: composable transformations of Python+NumPy programs, 2018. URL <http://github.com/google/jax>.
- Tianqi Chen, Ian J. Goodfellow, and Jonathon Shlens. Net2net: Accelerating learning via knowledge transfer. In *The Fourth International Conference on Learning Representations*, 2016. URL <http://arxiv.org/abs/1511.05641>.
- Zhao Chen, Vijay Badrinarayanan, Chen-Yu Lee, and Andrew Rabinovich. GradNorm: Gradient normalization for adaptive loss balancing in deep multitask networks. In Jennifer Dy and Andreas Krause, editors, *Proceedings of the 35th International Conference on Machine Learning*, volume 80 of *Proceedings of Machine Learning Research*, pages 794–803. PMLR, 10–15 Jul 2018. URL <https://proceedings.mlr.press/v80/chen18a.html>.
- Yaim Cooper. The loss landscape of overparameterized neural networks. *arXiv preprint arXiv:1804.10200*, 2018.
- Jacob Devlin, Ming-Wei Chang, Kenton Lee, and Kristina Toutanova. BERT: Pre-training of deep bidirectional transformers for language understanding. In *Proceedings of the 2019 Conference of the North American Chapter of the Association for Computational Linguistics: Human Language Technologies, Volume 1 (Long and Short Papers)*, pages 4171–4186, Minneapolis, Minnesota, June 2019. Association for Computational Linguistics. doi: 10.18653/v1/N19-1423. URL <https://aclanthology.org/N19-1423>.
- Arthur Douillard, Alexandre Ramé, Guillaume Couairon, and Matthieu Cord. Dytox: Transformers for continual learning with dynamic token expansion. In *Proceedings of the IEEE/CVF Conference on Computer Vision and Pattern Recognition*, pages 9285–9295, 2022.
- Rahim Entezari, Hanie Sedghi, Olga Saukh, and Behnam Neyshabur. The role of permutation invariance in linear mode connectivity of neural networks. *arXiv preprint arXiv:2110.06296*, 2021.
- Scott Fahlman and Christian Lebiere. The cascade-correlation learning architecture. In D. Touretzky, editor, *Advances in Neural Information Processing Systems*, volume 2. Morgan-Kaufmann, 1989. URL https://proceedings.neurips.cc/paper_files/paper/1989/file/69adc1e107f7f7d035d7baf04342e1ca-Paper.pdf.
- Pierre Foret, Ariel Kleiner, Hossein Mobahi, and Behnam Neyshabur. Sharpness-aware minimization for efficiently improving generalization. In *International Conference on Learning Representations*, 2021.
- Stanislav Fort, Gintare Karolina Dziugaite, Mansheej Paul, Sepideh Kharaghani, Daniel M Roy, and Surya Ganguli. Deep learning versus kernel learning: an empirical study of loss landscape geometry and the time evolution of the neural tangent kernel. *Advances in Neural Information Processing Systems*, 33:5850–5861, 2020.

- Jonathan Frankle, Gintare Karolina Dziugaite, Daniel Roy, and Michael Carbin. Linear mode connectivity and the lottery ticket hypothesis. In *International Conference on Machine Learning*, pages 3259–3269. PMLR, 2020.
- Timur Garipov, Pavel Izmailov, Dmitrii Podoprikin, Dmitry P Vetrov, and Andrew G Wilson. Loss surfaces, mode connectivity, and fast ensembling of dnns. *Advances in neural information processing systems*, 31, 2018.
- Andrea Gesmundo and Kaitlin Maile. Composable function-preserving expansions for transformer architectures. *arXiv preprint arXiv:2308.06103*, 2023.
- Linyuan Gong, Di He, Zhuohan Li, Tao Qin, Liwei Wang, and Tiejun Liu. Efficient training of BERT by progressively stacking. In Kamalika Chaudhuri and Ruslan Salakhutdinov, editors, *Proceedings of the 36th International Conference on Machine Learning*, volume 97 of *Proceedings of Machine Learning Research*, pages 2337–2346. PMLR, 09–15 Jun 2019. URL <https://proceedings.mlr.press/v97/gong19a.html>.
- Xiaotao Gu, Liyuan Liu, Hongkun Yu, Jing Li, Chen Chen, and Jiawei Han. On the transformer growth for progressive BERT training. In *Proceedings of the 2021 Conference of the North American Chapter of the Association for Computational Linguistics: Human Language Technologies*, pages 5174–5180, Online, June 2021. Association for Computational Linguistics. doi: 10.18653/v1/2021.naacl-main.406. URL <https://aclanthology.org/2021.naacl-main.406>.
- Steven Gutstein, Olac Fuentes, and Eric A. Freudenthal. Knowledge transfer in deep convolutional neural nets. *Int. J. Artif. Intell. Tools*, 17(3):555–567, 2008.
- Kaiming He, Xiangyu Zhang, Shaoqing Ren, and Jian Sun. Deep residual learning for image recognition. In *IEEE Conference on Computer Vision and Pattern Recognition*, 2016.
- Jared Kaplan, Sam McCandlish, Tom Henighan, Tom B Brown, Benjamin Chess, Rewon Child, Scott Gray, Alec Radford, Jeffrey Wu, and Dario Amodei. Scaling laws for neural language models. *arXiv preprint arXiv:2001.08361*, 2020.
- Simran Kaur, Jeremy Cohen, and Zachary Chase Lipton. On the maximum hessian eigenvalue and generalization. In *Proceedings on*, pages 51–65. PMLR, 2023.
- Rohith Kuditipudi, Xiang Wang, Holden Lee, Yi Zhang, Zhiyuan Li, Wei Hu, Rong Ge, and Sanjeev Arora. Explaining landscape connectivity of low-cost solutions for multilayer nets. *Advances in neural information processing systems*, 32, 2019.
- Daniel Kunin, Jonathan Bloom, Aleksandrina Goeva, and Cotton Seed. Loss landscapes of regularized linear autoencoders. In *International conference on machine learning*, pages 3560–3569. PMLR, 2019.
- Namhoon Lee, Thalaisyasingam Ajanthan, and Philip HS Torr. Snip: Single-shot network pruning based on connection sensitivity. *arXiv preprint arXiv:1810.02340*, 2018.
- Hao Li, Zheng Xu, Gavin Taylor, Christoph Studer, and Tom Goldstein. Visualizing the loss landscape of neural nets. *Advances in neural information processing systems*, 31, 2018.
- Lin Li and Michael Spratling. Understanding and combating robust overfitting via input loss landscape analysis and regularization. *Pattern Recognition*, 136:109229, 2023.
- Xilai Li, Yingbo Zhou, Tianfu Wu, Richard Socher, and Caiming Xiong. Learn to grow: A continual structure learning framework for overcoming catastrophic forgetting. *arXiv preprint arXiv:1904.00310*, 2019.
- Chaoyue Liu, Libin Zhu, and Mikhail Belkin. Loss landscapes and optimization in over-parameterized non-linear systems and neural networks. *Applied and Computational Harmonic Analysis*, 59: 85–116, 2022.
- Joe Mellor, Jack Turner, Amos Storkey, and Elliot J Crowley. Neural architecture search without training. In *International Conference on Machine Learning*, pages 7588–7598. PMLR, 2021.

- Stephen Merity, Caiming Xiong, James Bradbury, and Richard Socher. Pointer sentinel mixture models. *arXiv preprint arXiv:1609.07843*, 2016.
- Fidel A Guerrero Peña, Heitor Rapela Medeiros, Thomas Dubail, Masih Aminbeidokhti, Eric Granger, and Marco Pedersoli. Re-basin via implicit sinkhorn differentiation. In *Proceedings of the IEEE/CVF Conference on Computer Vision and Pattern Recognition*, pages 20237–20246, 2023.
- Llukan Puka. *Kendall’s Tau*, pages 713–715. Springer Berlin Heidelberg, Berlin, Heidelberg, 2011. ISBN 978-3-642-04898-2. doi: 10.1007/978-3-642-04898-2_324. URL https://doi.org/10.1007/978-3-642-04898-2_324.
- Yujia Qin, Cheng Qian, Jing Yi, Weize Chen, Yankai Lin, Xu Han, Zhiyuan Liu, Maosong Sun, and Jie Zhou. Exploring mode connectivity for pre-trained language models. *arXiv preprint arXiv:2210.14102*, 2022.
- Pengzhen Ren, Yun Xiao, Xiaojun Chang, Po-Yao Huang, Zhihui Li, Xiaojiang Chen, and Xin Wang. A comprehensive survey of neural architecture search: Challenges and solutions. *ACM Computing Surveys (CSUR)*, 54(4):1–34, 2021.
- Binxin Ru, Clare Lyle, Lisa Schut, Mark van der Wilk, and Yarin Gal. Revisiting the train loss: an efficient performance estimator for neural architecture search. *stat*, 1050:8, 2020.
- Robin Ru, Clare Lyle, Lisa Schut, Miroslav Fil, Mark van der Wilk, and Yarin Gal. Speedy performance estimation for neural architecture search. *Advances in Neural Information Processing Systems*, 34:4079–4092, 2021.
- Yu Shen, Yang Li, Jian Zheng, Wentao Zhang, Peng Yao, Jixiang Li, Sen Yang, Ji Liu, and Bin Cui. Proxybo: Accelerating neural architecture search via bayesian optimization with zero-cost proxies. In *Proceedings of the AAAI Conference on Artificial Intelligence*, volume 37, pages 9792–9801, 2023.
- Julien Siems, Lucas Zimmer, Arber Zela, Jovita Lukasik, Margret Keuper, and Frank Hutter. Nas-bench-301 and the case for surrogate benchmarks for neural architecture search. *arXiv preprint arXiv:2008.09777*, 4:14, 2020.
- Berfin Simsek, François Ged, Arthur Jacot, Francesco Spadaro, Clément Hongler, Wulfram Gerstner, and Johanni Brea. Geometry of the loss landscape in overparameterized neural networks: Symmetries and invariances. In *International Conference on Machine Learning*, pages 9722–9732. PMLR, 2021.
- Jost Tobias Springenberg, Aaron Klein, Stefan Falkner, and Frank Hutter. Bayesian optimization with robust bayesian neural networks. *Advances in neural information processing systems*, 29, 2016.
- Ruoyu Sun. Optimization for deep learning: theory and algorithms. *arXiv preprint arXiv:1912.08957*, 2019.
- Hidenori Tanaka, Daniel Kunin, Daniel L Yamins, and Surya Ganguli. Pruning neural networks without any data by iteratively conserving synaptic flow. *Advances in neural information processing systems*, 33:6377–6389, 2020.
- Ashish Vaswani, Noam Shazeer, Niki Parmar, Jakob Uszkoreit, Llion Jones, Aidan N Gomez, Łukasz Kaiser, and Illia Polosukhin. Attention is all you need. In *Advances in Neural Information Processing Systems*, 2017.
- Chaoqi Wang, Guodong Zhang, and Roger Grosse. Picking winning tickets before training by preserving gradient flow. *arXiv preprint arXiv:2002.07376*, 2020.
- Peihao Wang, Rameswar Panda, Lucas Torroba Hennigen, Philip Greengard, Leonid Karlinsky, Rogerio Feris, David Daniel Cox, Zhangyang Wang, and Yoon Kim. Learning to grow pretrained models for efficient transformer training. In *The Eleventh International Conference on Learning Representations*, 2023. URL <https://openreview.net/forum?id=cDYRS5iZ16f>.

- Xiang Wang, Annie N Wang, Mo Zhou, and Rong Ge. Plateau in monotonic linear interpolation—a "biased" view of loss landscape for deep networks. *arXiv preprint arXiv:2210.01019*, 2022.
- Colin White, Willie Neiswanger, and Yash Savani. Bananas: Bayesian optimization with neural architectures for neural architecture search. In *Proceedings of the AAAI conference on artificial intelligence*, volume 35, pages 10293–10301, 2021a.
- Colin White, Arber Zela, Robin Ru, Yang Liu, and Frank Hutter. How powerful are performance predictors in neural architecture search? *Advances in Neural Information Processing Systems*, 34: 28454–28469, 2021b.
- Colin White, Mahmoud Safari, Rhea Sukthanker, Binxin Ru, Thomas Elsken, Arber Zela, Debadeepta Dey, and Frank Hutter. Neural architecture search: Insights from 1000 papers. *arXiv preprint arXiv:2301.08727*, 2023.
- Thomas Wolf, Lysandre Debut, Victor Sanh, Julien Chaumond, Clement Delangue, Anthony Moi, Pierric Cistac, Tim Rault, Rémi Louf, Morgan Funtowicz, et al. Huggingface’s transformers: State-of-the-art natural language processing. *arXiv preprint arXiv:1910.03771*, 2019.
- Lei Wu, Chao Ma, et al. How SGD selects the global minima in over-parameterized learning: A dynamical stability perspective. *Advances in Neural Information Processing Systems*, 31, 2018.
- Yaoqing Yang, Liam Hodgkinson, Ryan Theisen, Joe Zou, Joseph E Gonzalez, Kannan Ramchandran, and Michael W Mahoney. Taxonomizing local versus global structure in neural network loss landscapes. *Advances in Neural Information Processing Systems*, 34:18722–18733, 2021.
- Chiyuan Zhang, Samy Bengio, and Yoram Singer. Are all layers created equal? *Journal of Machine Learning Research*, 23(67):1–28, 2022. URL <http://jmlr.org/papers/v23/20-069.html>.
- Zhangchen Zhou, Hanxu Zhou, Yuqing Li, and Zhi-Qin John Xu. Understanding the initial condensation of convolutional neural networks. *arXiv preprint arXiv:2305.09947*, 2023.
- Barret Zoph and Quoc Le. Neural architecture search with reinforcement learning. In *International Conference on Learning Representations*, 2017. URL <https://openreview.net/forum?id=r1Ue8Hcxg>.
- Barret Zoph, Vijay Vasudevan, Jonathon Shlens, and Quoc V Le. Learning transferable architectures for scalable image recognition. In *Proceedings of the IEEE conference on computer vision and pattern recognition*, pages 8697–8710, 2018.

A Appendix

A.1 Impact Statement

Large neural networks require substantial computational resources to be trained from scratch, and computing is not only finite but also expensive. Expanding smaller pre-trained models has the potential to make deep learning research quicker, more affordable, and more accessible to groups with limited resources. Furthermore, the large-scale infrastructures often required for training large models emit considerable amounts of carbon dioxide (CO₂). However, it is challenging to determine whether expansion would have a positive impact on the environment as, while it would help reduce the carbon footprint of each model, it would also allow training more models. Overall, we believe expansion is a step toward the re-usability of neural networks and, more generally, more sustainable deep learning.

A.2 Implementation Details and Additional Analysis

In this section, we provide the implementation details and results that were not included in the main content. In section A.2.1, we describe the process of generating permutation used in our experiments. In section A.2.2, we provide details about the datasets and models along with corresponding hyper-parameters values. Next, we provide a sensitivity analysis in section A.2.5 and a comparison between our method and the zero-cost baselines using different correlation metrics in section A.2.4. This is followed by additional experiments for analyzing the manifold size in an image classification task in section 4.3 and language modeling tasks in section A.2.7. We use the Jax library [Bradbury et al., 2018] in Python for our implementation. Experiments were conducted on NVIDIA V100 or A100 GPU machines with 32 GB and 40 GB memory, respectively.

A.2.1 Generating Random Permutations

As mentioned in section 4, we perform permutations on the neurons or channels of the first hidden layer in image classification tasks and the intermediate layer neurons of the first encode layer in the BERT models. For a given model, let θ represent the parameters located at a minimum. If the width of the first layer is l (≥ 4), we denote the corresponding input and output parameters of the first layer as the matrix θ_1^i with a shape of $x \times l$ and the matrix θ_1^o with a shape of $l \times y$. To permute the neurons in the layer in a function-preserving manner, we shuffle the columns of θ_1^i and the rows of θ_1^o using the same criteria. Since there are l neurons, there are $l!$ possible permutations that can be applied to obtain the same function.

The proposed metric requires finding edges through mode connectivity between minima. One might argue that swapping only two neurons in the layer can result in a closely located pair of minima. While this holds for smaller pre-trained models, employing this approach for larger base models may lead to a sample that only contains dead neurons. As a result, B_q^* can become very small, reducing the representative power of the manifold metric, as discussed in section 3. On the other hand, using entirely random permutations may result in generated minima located very far from each other. This is again not desirable since it will result in high loss barriers.

Therefore, as a trade-off between the distances between minima and the representative power of the metric, we iteratively sample $\lceil \log_2 l \rceil$ pairs of neurons and swap their position with replacement to obtain a new permutation. This way, the iteratively generated minima do not lie too far from one another in the loss landscape, making it easier to find edges between them.

A.2.2 Datasets and Models

In Table 1, we provide a summary of all datasets used in our experiments.

The tasks consist of:

- CIFAR10 is another multiclass image classification task whose training and validation sets consist of RGB images that are separated into 10 distinct classes, with each class containing an equal number of samples across the training and validation sets.
- CIFAR100 is similar to CIFAR10, except that images are now separated into 100 classes with an equal number of samples within each class.

Table 1: Dataset details

Dataset	Train Set	Validation Set	Input shape
CIFAR10	40K	10K	MLP: (3072); CNN: (32,32,3)
CIFAR100	40K	10K	(32, 32, 3)
WikiText-103	1.8M	3.76K	embedding dimension=128, sequence length=512

- WikiText-103 is a collection of over 100 million tokens extracted from the set of verified Good and Featured articles on Wikipedia. Since different articles, i.e., training samples, may have different lengths, the explicit size of the training and validation splits does not correspond to the number of training examples. Rather, this can be roughly estimated as the total number of tokens divided by the maximum sequence length, which is 512.

In Table 2, we provide the details about deep learning models and the levels of expansion performed in them. $F(\cdot)$ stands for the fully connected layer with a number of units in between parathesis. $C(\cdot)$ represents convolutional layers with the number of channels in between parathesis with a fixed kernel size of 3×3 . We expand the first convolutional layer in both CNNs used in our experiments in Figure 3 .

Table 2: Base models and expansion details for image classification tasks.

Model	Architecture	Expanded layers in candidate models
CNN (CIFAR10)	$C_1(8) - C_2(32) - MaxPool(2) - F_1(256)$	$\{C_1(10), C_1(12), C_1(16), C_1(24), C_1(32)\}$
CNN (CIFAR100)	$C_1(16) - C_2(64) - C_3(64) - C_4(64) - MaxPool(2) - F_1(256)$	$\{C_1(20), C_1(24), C_1(32), C_1(48), C_1(64)\}$

For the experiments in subsection 4.3.1, we expand (i) all the convolutional layers of CNN (CIFAR100) by width each with a given factor $\in \{1.25, 1.5, 2.0, 3.0\}$ and (ii) Add convolutional layers between $C_3(64)$ and $C_4(64)$. For the ResNet18 expansion, we increase the width of each convolutional layer present in the base model by a given factor $\in \{1.25, 1.5, 2.0, 2.5, 3.0\}$.

We followed the openly available MaskedLM BERT configuration in the language modeling experiments [Wolf et al., 2019]. The specific details of TinyBERT and MiniBERT are provided in Table 3. We perform expansion along the intermediate width of the FFN part in each encoder layer of the models. The widths in the candidate models are given in the final row in the table.

Table 3: Base models for language modeling tasks and expansion details.

	TinyBERT	MiniBERT
Number of attention heads	2	4
Number of encoder layers	2	4
Hidden dimension	128	256
Intermediate width	512	1024
Intermediate widths in expanded models	$\{640, 768, 1024, 1280\}$	$\{1152, 1280, 1536, 1792\}$

For the image classification task results shown in Figure 2, we used AdamW optimizer with a learning rate of 0.001, weight decay of 0.0001, and beta values (0.9, 0.999) to obtain the pre-trained models. The batch size was fixed to 512 for CIFAR10 and CIFAR100. For language modeling tasks, we used Adam optimizer with the learning rate 0.0003 and beta values (0.9, 0.999). We use a cosine learning rate scheduler with a warmup of 1000 steps. The batch size was fixed at 8 per GPU core for training. We compute the manifold metric and zero-cost baselines on a single batch of the training dataset and show the zero-cost correlation obtained for the metrics across all the tasks.

For the rest of the experiments described in section 4.3 and section 4.4, we fixed the pre-trained base model ϕ^* obtained using early-stopping criteria. We perform the expansion as described in the previous section and train the model to analyze how manifold size evolves. This is done by storing checkpoints at multiple epochs and computing the metrics across them.

We show the manifold metric results obtained from the best-performing hyper-parameter setup by performing a grid search over different threshold quantiles q and the number of nodes n . For

grid search over q , we use the set $Q = \{0.05, 0.1, 0.2, 0.4\}$, and for n , we use the set $N = \{50, 100, 250, 500, 1000\}$. Note that, to reduce computation time, we do not run the algorithm 1 separately for each combination (q, n) . Instead, we obtain the set $B^* = \{\hat{b}_i(\phi^*) : i \in [1, \max_{\eta} N]\}$, and compute the B_q^* from the subset $B^*[1 : n]$ for $q \in Q$ and $n \in N$ where $[\cdot]$ represents slice of the set given the indices. Therefore, the computation requirement for hyper-parameter search is proportional to the maximum value in N .

A.2.3 Baselines

We compare our manifold metric with the following NAS baselines used in [White et al., 2021b]. Our implementation of these baselines in Jax is based on the code made available by [Mellor et al., 2021].

- GradNorm [Abdelfattah et al., 2021]: It is the sum of the Euclidean norm of the gradients of one minibatch of training data. This measure is an indication of the property of loss landscape.
- Jacov [Mellor et al., 2021]: It is the covariance of the Jacobian of the model’s prediction with respect to the input. It involves computing the highest eigenvalue of the covariance matrix.
- SNIP [Lee et al., 2018]: Single-shot network pruning (SNIP) is a network pruning method that involves masking the parameters and running a backward pass.
- Grasp [Wang et al., 2020]: Gradient signal preservation is a network pruning method that involves computing a Hessian vector product.
- SynFlow [Tanaka et al., 2020]: Synaptic Flow is another network pruning method that involves a backward pass and a vector-vector product computation.
- SoTL-E [Ru et al., 2021]: It is the sum of the training losses in the most recent epoch. Unlike other baselines which are zero-cost proxies, it requires training the model and is therefore significantly more expensive.

Table 4 compares our manifold metric against the other above-mentioned zero-cost proxies. The metrics efficiency is measured as the time (in seconds) to compute them on a checkpoint immediately after expansion with the highest factor for different image classification setups. Since the manifold metric does not require a backward pass but rather performs multiple forward passes, it is computationally more efficient than the baselines. The efficiency holds when the model complexity increases from CNN to ResNet18. Notably, the manifold metric is faster than the second-best baseline, SynFlow.

Table 4: Comparison between our manifold metric with zero-cost baselines based on computation involved and the actual time taken (in seconds) on a given checkpoint using a single batch of data. * indicates that gradients are computed with respect to the outputs instead of loss.

Method	Number of forward passes	Highest derivative order	Time taken (seconds)		
			CNN (CIFAR10)	CNN (CIFAR100)	ResNet18
GradNorm	1	1	0.4 ± 0.01	0.5 ± 0.01	4.4 ± 1.1
Jacov	1	1*	0.4 ± 0.01	0.6 ± 0.01	2.8 ± 0.7
SNIP	1	1	0.4 ± 0.02	0.5 ± 0.01	3.8 ± 1.0
Grasp	1	2	0.5 ± 0.01	0.7 ± 0.02	6.4 ± 1.5
SynFlow	1	1*	0.6 ± 0.11	0.7 ± 0.13	4.4 ± 1.2
Manifold (ours)	$2n + 1 (= 101)$	0	0.4 ± 0.01	0.6 ± 0.01	2.1 ± 0.5

A.2.4 Rank Correlation Metrics

In this section, we provide a comparison between the manifold metric and the zero-cost baselines in terms of Spearman rank correlation and Pearson rank correlation. We plot the results in Figure 7. In both cases, we observe the same trend as Figure 2 where, unlike the baselines, the correlation between the manifold metric and the performance gain remains positive across different models and datasets, and other baselines.

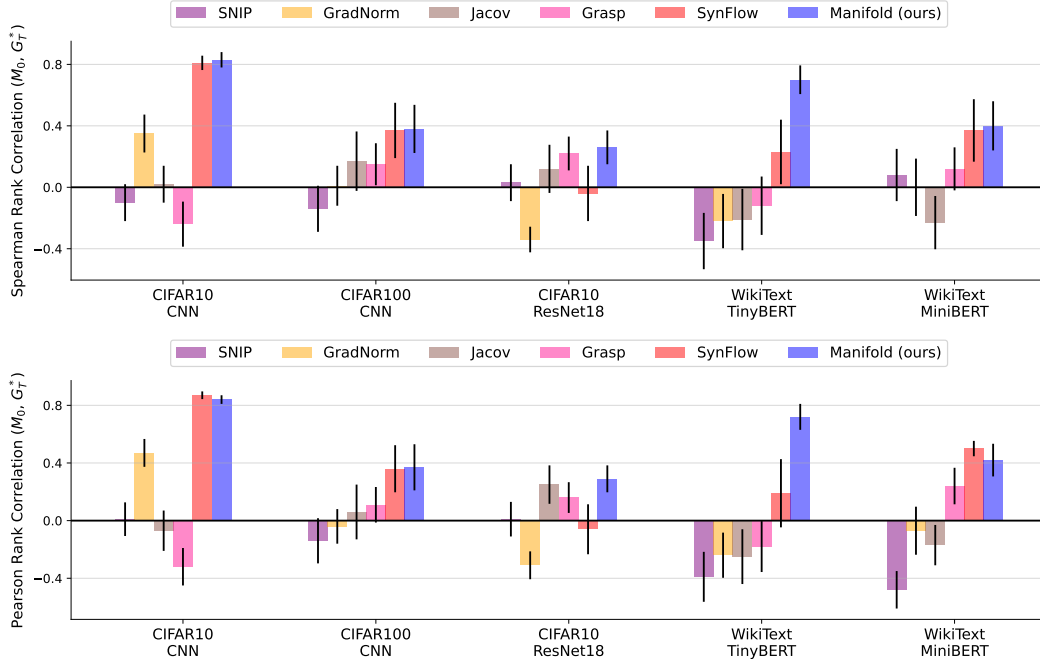


Figure 7: Comparison between the manifold metric M_0 and the existing zero-cost proxies in terms of Spearman rank correlation (top) and Pearson rank correlation (bottom) with G_T^* (final performance gain). The horizontal axis notes the dataset and the base model. M_0 correlation remains consistently positive, whereas baselines exhibit both positive and negative correlations similar to Figure 2.

A.2.5 Sensitivity Analysis

This section presents additional sensitivity analysis results obtained by performing a grid search over the hyperparameters q and n as defined in the previous section. We calculate the Kendall Tau correlation between the manifold metric and the final performance gain for various combinations of (q, n) . Figure 8 illustrates the average correlation obtained from ten seeds for CIFAR100 and MiniBERT experiments. We observe that there is not any clear trend in the case of CIFAR100 due to low overall correlation, unlike CIFAR10 in Figure 6. On the other hand, the MiniBERT correlation remains high for a larger number of permutations n and threshold quantile q in the case of MiniBERT.

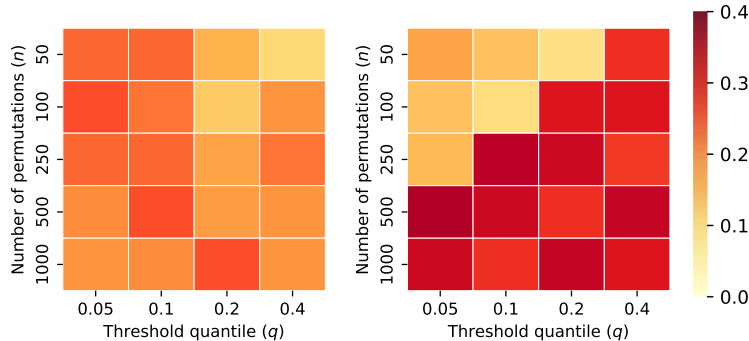


Figure 8: Sensitivity analysis on CNN on CIFAR100 (first) and MiniBERT on WikiText-103 (second), in terms of Kendall Tau correlation observed between the manifold metric M_0 and the overall performance gain G_T^* . We observe that the correlation is low but positive for CIFAR100. On the other hand, it increases as we grow the number of permutations n and threshold quantile q in MiniBERT.

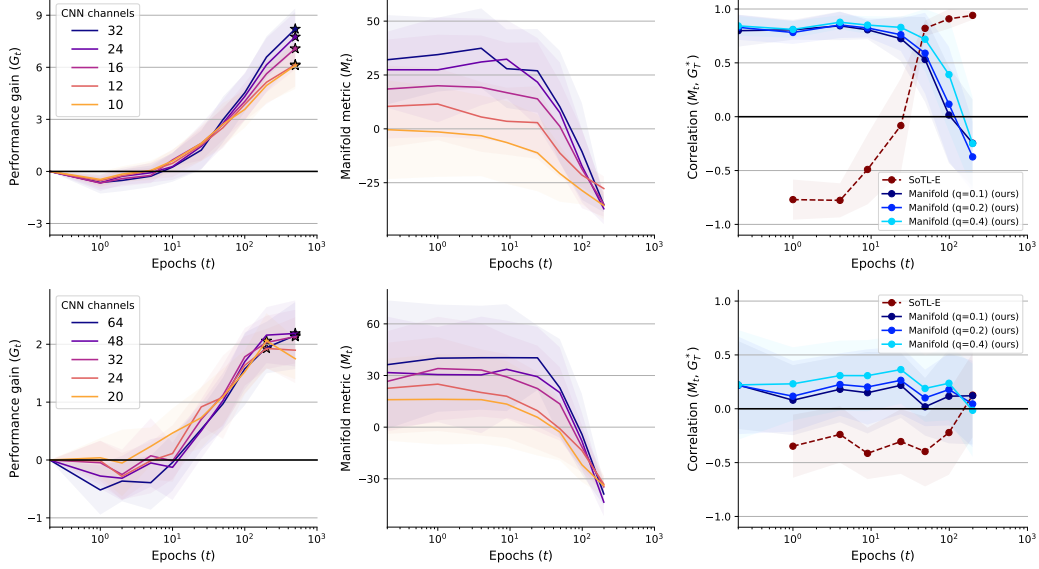


Figure 9: Performance gain G_t (first column; \star denotes the best performance gain G_T^*), manifold metric M_t (second column) and correlation between M_t and the highest gain G_T^* (third column) on expanding and training CNN on CIFAR10 (top) or CIFAR100 (bottom) for $T = 500$ epochs when a model is pre-trained using Adam optimizer. Similar to Figure 3, M_t remains constant and proportional to G_T^* from the beginning and drops during the later stages of training.

A.2.6 Training CNN with Adam

Earlier in subsection 4.3, the results were obtained when the expanded CNN models were trained using the AdamW optimizer. In this section, we run similar experiments but train the CNN models using the Adam optimizer to investigate how weight decay affects the manifold of the loss landscape during the training process.

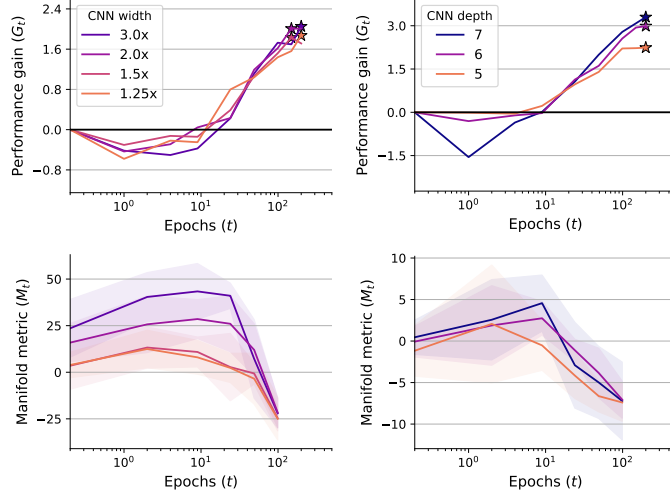


Figure 10: Performance gain G_t (first row; \star denotes the best performance gain G_T^*) and manifold metric M_t (second row) for CNN width expansion for all layers (first column) and CNN depth expansion on CIFAR100 (second column) using Adam optimizer. The manifold metric M_t positively correlates with the level of expansion initially. However, we also observe a quicker drop for M_t in case of depth expansion.

The corresponding results shown in Figure 9 and Figure 10 have a similar trend as the AdamW experiments. However, we also observe a quicker drop for M_t in case of large expansion factors during the later training phase. Thus, we conclude that the manifold metric is robust toward the use of weight decay in capturing geometric properties of the loss landscape, especially in the initial phase which is more desirable to evaluate model expansion.

A.2.7 Additional Experiments for Transformer

We provide the results of ablation experiments for analyzing how manifold size changes in a Transformer.

We train a Transformer from a random initialization for 10 epochs. The manifold size at initialization should be vast due to parameters lying on a high-loss surface. Therefore, to compute M_t , we use the manifold size at epoch 1 as a reference point and monitor how it changes during training. We compare the metric M_t across different q and plot them in Figure 11 (first). We observe that in all cases, the manifold size decreases. Moreover, the drop grows with q , suggesting that even the non-linear mode connectivity between parameters drops as the model is trained.

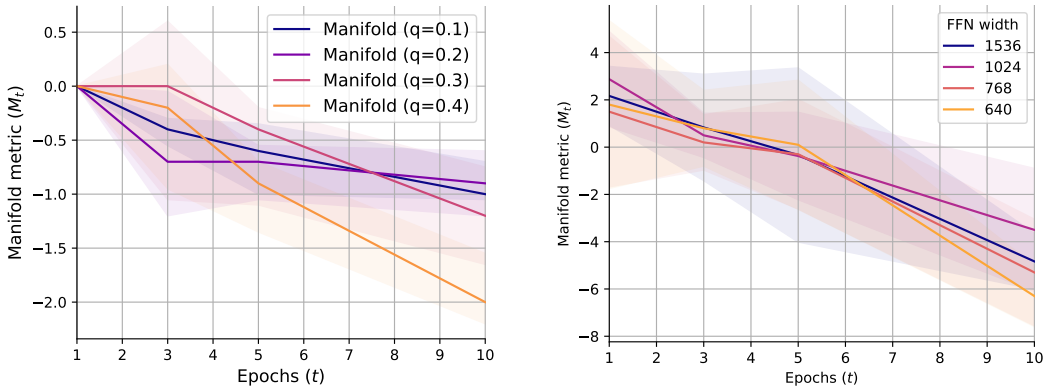


Figure 11: (i) Comparing manifold size while training TinyBERT on WikiText-103 for $T = 10$ epochs starting from random initialization. Similar to Figure 5, the manifold size drops as the model is trained further. (ii) Manifold metric M_t computed by permuting self-attention weights during training TinyBERT model on WikiText dataset. The manifold size decreases as the model is trained similar to Figure 5.

In another experiment, we permute self-attention layer weights instead of FFN weights of the first encoder layer in TinyBERT to obtain different minima. Figure 11 (second) shows the manifold metric obtained during training different expanded models. We observe that the manifold size decreases throughout training similar to Figure 5 (middle). This ablation experiment also suggests that the manifold metric does not depend on the type of permutation applied to this model to obtain different minima.